Minerals Engineering 203 (2023) 108363

Contents lists available at ScienceDirect

Minerals Engineering

journal homepage: www.elsevier.com/locate/mineng

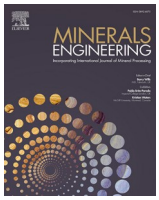

# Selective sequential extraction and microanalysis for revealing distribution, occurrence mode, and removal potential of arsenic in phosphate ore

Guiyong Zhou [a,b], Ning Wang [a], Wei Xu [c], Guotao Hu [c], Hannian Gu [a,b,*]

[a] Key Laboratory of High-temperature and High-pressure Study of the Earth's Interior, Institute of Geochemistry, Chinese Academy of Sciences, Guiyang 550081, China
[b] University of Chinese Academy of Sciences, Beijing 100049, China
[c] Wengfu (Group) Co., Ltd., Guiyang 550002, China

ARTICLE INFO

*Keywords:*
Phosphate ore
Arsenic
Occurrence mode
Iron oxides/hydroxides
Pyrite

ABSTRACT

Arsenic (As) is a common impurity extensively existing in phosphate ore and it has to be removed using complicated operations during the phosphorus chemical process. To investigate the occurrence mode of As would be beneficial to evaluate the separation of As from phosphate ore in the flotation process. In the current study, selective sequential extraction (SSE) and microanalysis were employed to reveal the distribution and occurrence modes of As in a phosphate ore sample. The SSE results indicated that As in the phosphate ore was dispersed in fractions of carbonate minerals (18.27 %), oxides/hydroxides (ca. 38 %), and sulfide minerals (22.07 %). In addition, 3.05 % of As could be extracted in the exchangeable and soluble fraction. Microanalysis of scanning electron microscope (SEM), transmission electron microscope (TEM), and electron probe micro-analyzer (EPMA) revealed the main arsenic-containing minerals by means of energy dispersive spectrometer (EDS) or wavelength dispersive spectrometer (WDS). Results showed that all of iron oxides/hydroxides phases, all of rhodochrosite particles, and parts of pyrite were arsenic-containing, with the average contents of As measured to be 0.142, 0.052, and 0.047 %, respectively. Consequently, arsenic amounts in the phosphate ore descended in the order of iron oxides/hydroxides > pyrite > rhodochrosite. These arsenic-containing minerals/phases could be removed through different beneficiation methods, such as flotation and chemical minerals processing. The findings of this study provide a mineralogical insight into developing potential techniques to remove As from phosphate ores.

## 1. Introduction

Phosphate ore is an important non-renewable resource, and its downstream phosphorus chemical products have a wide range of applications in agriculture, chemical, food, etc. (Yang and Guan, 2023). The global phosphate ore reserves are around 50 billion tons, principally occurring as sedimentary phosphorites (USGS, 2022). China has the second largest phosphate reserves in the world (USGS, 2022), among which the phosphate ore is mainly in the form of medium–low grade with an average grade of mere 17 % ($P_2O_5$) (Jiang, 2014). In the southwest of China, a large sedimentary phosphate deposit is located in the Doushantuo Formation of Lower Sinian system (Ren et al., 2015) and it can be divided into high-grade phosphate ore and medium–low-grade phosphate ore. The high-grade part has been widely used in the industry to manufacture phosphorus chemical products, and there has been limited exploitation of the medium–low grade ores because of the high impurities contents (Dong et al., 2021). It is expected to be depleted around 2033 due to high-grade phosphate ore constant consumption (Elser, 2012). Hence, there has been widespread interest in how to effectively use medium–low grade phosphate ore resources (Aarab et al., 2021; Dong et al., 2021). To exploit medium–low-grade phosphate ore has to focus on the impurities elements inside.

Arsenic (As) is an impurity element that extensively existed in phosphate ore (Stow, 1969), and it can be further enriched in phosphorus chemical products. For example, if the As content in phosphate ore exceeds 10 mg/kg, it will be as high as 140–150 mg/kg in the yellow phosphorus product, which belongs to the worst grade of yellow phosphorus product (Ni et al., 1997). In particular, the standard of As content in high purity phosphoric acid which is widely used in manufacturing electronic grade phosphoric acid is strictly limited to less than 1 mg/kg (Wang and Luo, 2014). Otherwise, As affects the concentration of electrons and holes in silicon during the semiconductor etching process,

* Corresponding author at: Key Laboratory of High-temperature and High-pressure Study of the Earth's Interior, Institute of Geochemistry, Chinese Academy of Sciences, Guiyang 550081, China.
*E-mail address:* guhannian@vip.gyig.ac.cn (H. Gu).

https://doi.org/10.1016/j.mineng.2023.108363
Received 19 June 2023; Received in revised form 29 August 2023; Accepted 3 September 2023
Available online 8 September 2023

leading to a decrease in the quality of semiconductor products (Wen, 1992). Hence, the As content is an important criterion for classification of phosphate ore, with levels greater than 10 mg/kg being considered high-arsenic phosphate ore (Ni et al., 1997). Arsenic contains strong biotoxicity under long-term exposure, which may cause muscle cramping, cardiovascular disease, and cancer (Islam et al., 2023). The occurrence mode of As in phosphate ore dictates its mobility and probably results in the potential release into products and the surrounding environment, leading to a threat to human health and a source of environmental pollution (Benredjem and Delimi, 2009). In addition, As in the phosphorus chemical industry by-product (phosphogypsum) also has been on the list of potentially toxic elements of the Environmental Protection Agency (Curran and Lopez, 2021; Wu et al., 2022). Therefore, As content is an important restriction factor limiting the development of phosphorus industrial products to a high value-added direction.

Currently, As removal from phosphoric acid is a necessary process by means of flotation, adsorption, and precipitation (Bahsaine et al., 2022). The precipitation method by adding $Na_2S$ to wipe off As is widely applied for the production of high-purity phosphoric acid (Bahsaine et al., 2022; Daryani et al., 2022). However, the current As removal process is complex and will introduce $Na^+$ impurities to the products (Li et al., 2020). Hence, the characterization of As mineralogical residence is vital when developing diverse and simple techniques to remove As in the phosphorus chemical industry.

Associated As with the rock components of phosphate ore has received research attentions (Stow, 1969; Baioumy, 2005). Correlation analysis methods were employed to investigate the occurrence mode of As in phosphate ore, and the findings indicated that iron oxide is the principal component correlated with the abundance of As for Florida land-pebble phosphate rocks (Stow, 1969), while for phosphorites in Egypt, As was suggested to be in the form of sulfides because of strong positive correlation between As and sulfur (Baioumy, 2005). Arsenic also was thought to be related to pyrite, iron oxides, and organic components in phosphate ores (Lazareva and Pichler, 2009). To sum up, the previous works were mainly based on geochemical correlation of elements, and revealing the specific occurrence minerals of As and quantitative analysis of As distribution in phosphate ore needs further investigation.

The present study aims to provide accurate results regarding the mineralogical residence of As in phosphate ore. An arsenic-rich phosphate ore was selected and characterized for its mineral composition. Selective sequential extraction (SSE) procedure was applied for revealing As distribution in diverse fractions. Meanwhile, several microanalysis methods were carried on to identify arsenic-containing minerals. The findings of this work can be useful for forecasting the migration rule of As in the phosphorus chemical industry and providing guidance for the removal of As from phosphate ore in the future.

## 2. Materials and methods

### 2.1. Samples and reagents

The phosphate ore used was collected from a dressing plant of Wengfu Group, which was stacked for beneficiation processing. It was derived from Chuanyandong ore of Wengfu open-cast mining, Weng'an County, Guizhou, China. The sample was dried at 40 °C for 24 h in a drying baker. Afterward, the sample with large blocks was ground using agate mortar in the laboratory and was then sieved through 0.074 mm before characterizations and experiments. Reagents of $NH_4NO_3$ (ammonium nitrate), $NH_3{\cdot}H_2O$ (ammonium hydroxide), $CH_3COOH$ (acetic acid), $(NH_4)_2C_2O_4$ (ammonium oxalate), $C_6H_8O_6$ (ascorbic acid), and $HNO_3$ (nitric acid) were of analytical grade and were used to prepare extraction solutions. Deionized water (18.25 MΩ) was used for the preparation of extracted solutions and the washing steps of selective sequential extraction (SSE).

### 2.2. Selective sequential extraction

Selective sequential extraction is an effective method to investigate the occurrence mode of elements, assuming that the elements in different phases can be dissolved by different reagents without affecting the other phases. It was originally developed for the analysis of the occurrence state of elements in soil (Tessier et al., 1979) and was then developed with modification for coal and shale samples (Wenzal et al., 2001; Dai et al., 2004; Goren, 2015). The method has since been refined to better suit the research on the occurrence state of the elements in sedimentary minerals (Goren, 2015; Yang et al., 2016; Liu et al., 2018). Since phosphate ore belongs to sedimentary mineral resources, the SSE process can be used to investigate the occurrence of elements in phosphate ore.

The SSE procedure included five sequential steps to distinguish six fractions as shown in Table 1. Particularly, carbonate minerals (CARB) were usually identified by dissolution using 1 M NaOAc solution at pH of 4 (Goren, 2015). In this study, to dissolve large amounts of dolomite in phosphate ore, the present SSE procedure used 6 % of acetic acid solution to substitute NaOAc for CARB fraction identification. The XRD comparison of before and after acetic acid leaching is shown in Fig. 1a, and the results illustrated that the dolomite in phosphate ore could be dissolved well.

The SSE procedure began with adding 1.0 g of dried and homogenized sample into a 50 mL polypropylene centrifuge tube. In each of the five initial steps, 25 mL of the extraction reagent was added to the residual sediment obtained from the previous step. In general, the tubes were positioned horizontally to achieve maximal solid-solution interaction. The mixture was shaken for the time and temperature determined (Table 1). After each extraction step, the tube containing phosphate ore and extraction leachate was centrifuged at 3500 rpm for 10 min. Furthermore, the solution entrapped in the remaining samples was collected in subsequent washing steps and combined with the corresponding extract. The final insoluble residue was insoluble residue fraction (IR) and was dried for elemental determination. Each SSE step was conducted in triplicate to effectively reduce the experimental error and the results presented were the average values of three replicate.

**Table 1**
Detail steps of the sequential extraction procedure used in this study.

| Steps | Fractions | Reagents | Extraction conditions | Washing steps |
|---|---|---|---|---|
| 1 | Exchangeable and soluble (EXC)[b] | 1 M $NH_3NO_3$ ($NH_3{\cdot}H_2O$, pH = 7) | 30 min shaking, 20 °C, S/L[a] = 1:25 | Deionized water; 10 min shaking; S/L 1:12.5; two times |
| 2 | Carbonate minerals (CARB) | 6 % $CH_3COOH$ | 4 h shaking, 20 °C, S/L = 1:25 | Deionized water; 10 min shaking; S/L 1:12.5; two times |
| 3 | Amorphous oxides (AO)[c] | 0.2 M $(NH_4)_2C_2O_4$ | 4 h shaking in the dark, 20 °C, S/L = 1:25 | $(NH_2)_2C_2O_4$ (0.2 M); S/L 1:12.5; 10 min shaking in the dark; two times |
| 4 | Crystalline oxides (CO)[c] | 0.2 M $(NH_4)_2C_2O_4$ (ascorbic acid, pH = 3.25) | 30 min in a water basin at 96 ± 3 °C in the light, S/L = 1:25 | $(NH_2)_2C_2O_4$ (0.2 M); pH 3.25; S/L 1:12.5; 10 min shaking in the dark; two times |
| 5 | Sulfide minerals (SM)[d] | 65 % $HNO_3$ | 2 h shaking, 80 °C, S/L = 1:25 | Deionized water; 10 min shaking; S/L 1:12.5; two times |

[a] S/L: solid-to-liquid ratio, g/mL.
[b] Groen (2015).
[c] Wenzal et al. (2001).
[d] Dai et al. (2004).

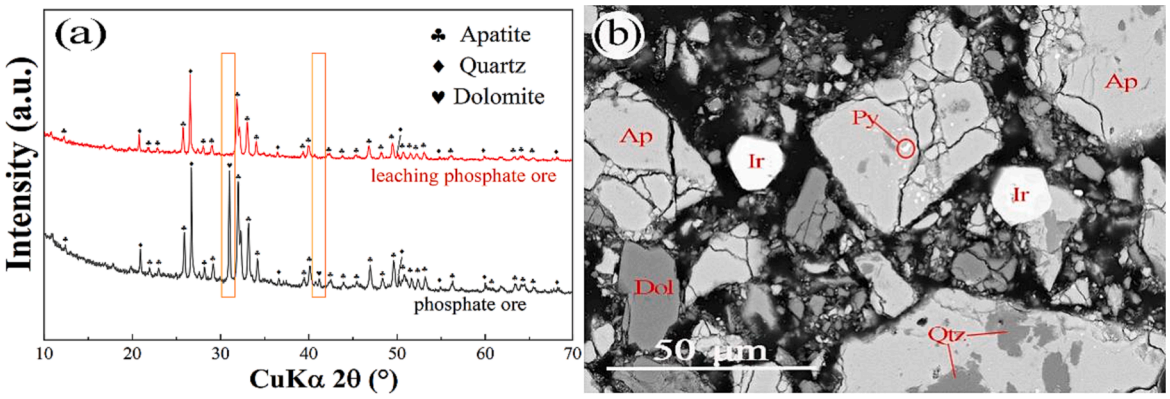


**Fig. 1.** (a) XRD comparison of the raw phosphate ore and after CARB leaching using 6 % acetic acid solution and (b) SEM backscatter image of the phosphate ore, Ap-apatite, Dol-dolomite, Qtz-quartz, Py-pyrite, Ir-iron oxides/hydroxides.

### 2.3. Characterization methods

The main chemical compositions of the phosphate ore were determined by X-ray fluorescence spectroscopy (XRF, PANalytical PW2424, Netherlands). A prepared sample of XRF was fused with a lithium metaborate-lithium tetrabo-rate flux which also included an oxidizing agent (lithium nitrate) and was then poured into a platinum mold. After that, the obtained disk was analyzed by XRF spectrometry. The XRF analysis was examined in conjunction with a loss-on-ignition (LOI) at 1000 °C, and the resulting data came from the combination of the two methods. X-ray diffraction spectroscopy (XRD, PANalytical Empyrean, Netherlands) was used to identify the mineral compositions of the phosphate ore. The XRD patterns of the samples were recorded utilizing Cu Kα radiation. The apparatus was conducted under standard conditions at 40 kV, 20 mA. The XRD spectra were scanned at a 2θ range from 5° to 60° at a speed of 10°/min, with a step length of 0.03°.

The scanning electron microscope (SEM) images of samples were observed by a Scios (FEI, USA) field emission scanning electron microscope with an energy dispersive spectrometer (EDS). The EDS was worked with an operating voltage of 20 kV and an operating current of 1.6nA, and the spot size was 2 nm. The samples were made flakes before grinding and after, and observed under SEM after pre-treatment such as carbon spray, with a working distance of 5.3 mm. The transmission electron microscope (Tecnai G2 F20 S-Twin, USA) with an energy dispersive spectrometer (TEM-EDS) was used for morphology and element analysis of the phosphate ore particles. The EDS was worked with an accelerating voltage of 20 kV and beam current of 1 nA. Approximately 1 g sample was dispersed into ethyl alcohol suspension for 5 min using an ultrasonic disperser, and a droplet of the sample dispersion was then dropped onto a lacy carbon-coated 20-mesh Cu grid and transferred to the microscope for observation after drying. The electron probe micro-analyzer (EPMA) element analysis of samples was determined by a JXA-8530F (JEOL, Japan) field emission electron probe micro-analyzer with wavelength dispersive spectrometer (WDS). Analyses were performed at 25 keV acceleration potential and 2 μA beam current. As reference materials magnetite ($Fe_3O_4$), pyrite ($FeS_2$), pyrope ($Mg_3Al_2(SiO_4)_3$), FeAsS, and Mn were used. In addition, mineral identification in phosphate ore was conducted using TESCAN Integrated Mineral Analyzer (TIMA, TIMA X, Czech Republic). It consists of the combination of a Scanning Electron Microscope with four light-element energy-dispersive X-ray spectroscopy (EDS) detectors. The EDS data are used to classify the analyzed point based on a database of known mineral compositions, therefore inferring the mineralogy at each point in a systematically scanned image of a sample and obtaining the classification, abundance, and distribution of minerals.

The element concentrations of the solution and insoluble residue after SSE were determined by inductively coupled plasma-atomic emission spectrometry (ICP-AES, Agilent VISTA, USA). The solid samples were first pre-oxidised with nitric and perchloric acids to convert As to pentavalent As to reduce volatilisation. Hydrofluoric acid was then added and the reaction was heated on an electric furnace. The residual solution was diluted with hydrochloric acid and fixed, and then analysed by plasma emission spectroscopy. The liquid samples are tested directly by acidizing, and the liquid is concentrated or diluted if the value of the element measured is low or above the detection limit of the instrument. Spectral interferences between elements are corrected and the final analytical result is obtained.

## 3. Results and discussion

### 3.1. Characterization of phosphate ore

The main chemical composition of the phosphate ore is shown in Table 2, and the chemical composition of $P_2O_5$, $CaO$, and $SiO_2$ in the phosphate ore are the dominant components, accounting for 24.10, 36.40, and 18.96 %, respectively. Such chemical compositions indicate the phosphate ore belongs to a medium–low-grade phosphate ore with high silicon content (Wang et al., 2022). The trace element concentrations of the phosphate ore are shown in Table 3, and the As content of the phosphate ore is 43.8 mg/kg. It should be classified as a high-arsenic phosphate ore because the As content is higher than 10 mg/kg (Ni et al., 1997).

SEM backscatter image further revealed the grain size and embedded features of the minerals in the phosphate ore sample as shown in Fig. 1b and S1. Combined with XRD analysis results (Fig. 1a), the main phases of the phosphate ore were recognized as apatite, dolomite, and quartz, with small amounts of pyrite, iron oxides/hydroxides. It also can be observed that the sizes of apatite were a bit larger than those of dolomite. Quartz was mostly embedded in the apatite particles. Pyrite particles embedded in apatite while iron oxides/hydroxides existed independently with good granular crystal shapes.

### 3.2. The dissolution and distribution of arsenic

#### 3.2.1. Evaluation of effectiveness of the SSE method

The recovery of the different elements in the SSE was calculated by the ratio of the total of SSE contents and the total contents measured by ICP-AES or XRF. The recovery values of all elements in this study ranged from 78 to 102 % (Table S1), and the range of 100 ± 40 % for SSE could be acceptable (Goren, 2015). Fig. 2 shows the distribution of Mg, Fe, S, and Si among the six fractions of SSE in the phosphate ore. In the CARB fraction, approximately 60 % of Mg was extracted (Fig. 2a) due to the dissolution of dolomite implying a good selectivity of using acetic acid to obtain CARB fraction from phosphate ore. Sulfur in phosphate ore was reported mainly occurred as sulfides, especially as pyrite. The proposed SSE procedure suggested that more than 70 % of S was released in the

**Table 2**
Main chemical composition of the phosphate ore (wt %).

| Components | CaO | $P_2O_5$ | $SiO_2$ | MgO | $SO_3$ | $K_2O$ | $Fe_2O_3$ | $Al_2O_3$ | MnO | $Na_2O$ | LOI |
|---|---|---|---|---|---|---|---|---|---|---|---|
| Content | 36.40 | 24.10 | 18.96 | 2.44 | 2.17 | 1.96 | 1.79 | 4.69 | 0.27 | 0.01 | 6.27 |

**Table 3**
Trace element including concentrations of the phosphate ore (mg/kg).

| Elements | As | Ga | Zr | Ta | V | Th | Sr | Hf | Rb | Zn | REEs[a] | U | Ni |
|---|---|---|---|---|---|---|---|---|---|---|---|---|---|
| Content | 43.8 | 6.99 | 67 | 0.2 | 28 | 4.51 | 834 | 1.5 | 34.9 | 14 | 246.5 | 9.61 | 16 |

[a] REEs: rare earth elements including scandium, yttrium, and lanthanide.

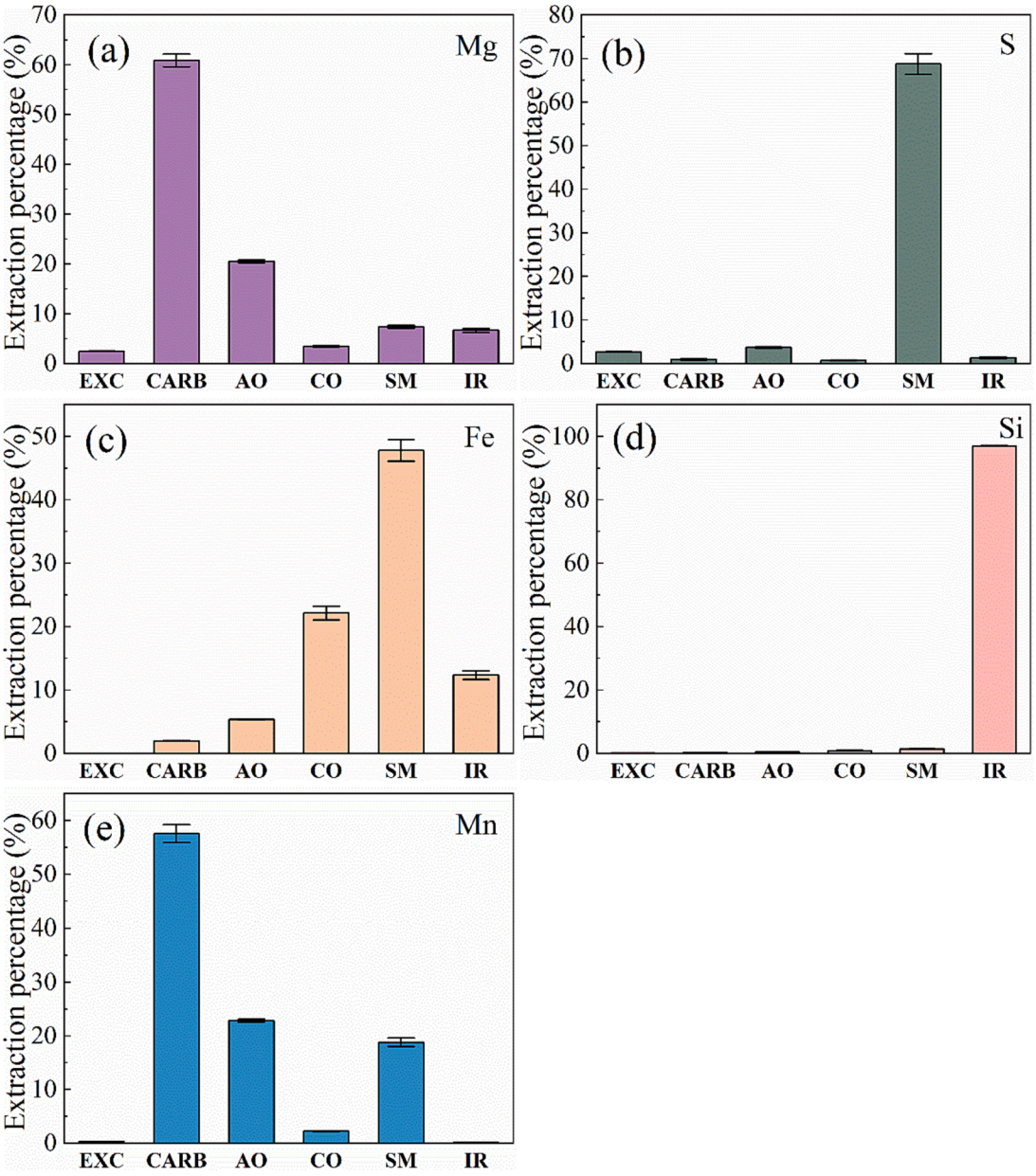


**Fig. 2.** Distribution of typical elements of (a) Mg, (b) S, (c) Fe, (d) Si, and (e) Mn in the phosphate ore from SSE extraction steps.

SM fraction (Fig. 2b). The releasing of Fe in the SM fraction was merely 50 % as shown in Fig. 2c. The results could be attributed to the existing of both iron oxides and iron hydroxides as shown in Fig. 1b. The remaining of Si in the IR fraction accounted for approximately 95 % as shown in Fig. 2d, which indicated that clay minerals could not be dissolved in the first four steps. According to the above analysis for the extraction distribution of Mg, Fe, S, and Si, it can be concluded that the SSE procedure can dissolve the corresponding components well for the

phosphate ore, and it could be used to investigate the distribution of As in the phosphate ore.

### 3.2.2. Distribution of arsenic

The distribution of As in the five extraction steps from the SSE is presented in Fig. 3. Totally, dissolution of As in AO and CO fractions (the total oxides/hydroxides fraction) accounted for the highest proportion of a little more than 38 %, followed by SM and CARB fractions.

**Exchangeable and soluble fraction (EXC).** Generally, EXC fraction of the SSE represents the elements with weak bonds. More than 3 % liberating of As was obtained during the extraction process from the vigorous shaking, indicative the probable existence of the adsorption of As on the particle surfaces of the phosphate ore. Arsenic can be adsorbed on original clays and Mn/Fe oxides/ hydroxides in sediments (Doušová et al., 2011; Mirlean et al., 2012), and these substances also widely exist in phosphate ores. The current results have not been able to determine the specific minerals that the As is attached to. However, the EXC fraction As would be easier released into the phosphoric acid solution when the phosphate ore is subjected sulfuric acid leaching in the phosphorus chemical industry.

**Carbonate minerals fraction (CARB).** In the CARB fraction, the extraction rate of Mn was close to 60 % (Fig. 2e), implying the existence of manganese carbonate minerals, though Mn usually occurs in phosphorite in oxides forms (Gál et al., 2020). Another carbonate dolomite was determined without As contained (Fig. S2). Thus, 18.27 % of As dissolution was attributed to the Mn-containing carbonate minerals, which was also demonstrated from the microanalysis as detailed below.

**Amorphous oxides (AO) and crystalline oxides (CO) fractions.** AO and CO fractions constitute the total oxides/hydroxides fraction of a particular element. The As dissolution in the total oxides/hydroxides fraction was as high as 38.04 %, and this was mainly due to iron dissolution. Consequently, the iron oxides/hydroxides were one of the main arsenic-rich phases in the phosphate ore. Previous research had also confirmed the presence of As in phosphate ore mainly in iron oxides (Stow, 1969), herein, iron oxides/hydroxides were used because the SSE procedure and EDS/WDS analyses cannot differentiate oxides and hydroxides. The occurrence mode of As in iron oxides/hydroxides will also be discussed in the microanalysis section below.

**Sulfide minerals fraction (SM).** In the SM fraction, the content of As was 22.07 %, and iron also had a high extraction rate of nearly 50 % (Fig. 2c). These results suggested that As was related to sulfide minerals and iron-containing minerals in the phosphate ore. The presence of As in pyrite has been widely known (Qiu et al., 2017; Zhao et al., 2021). However, other arsenic-containing sulfide minerals that might be present in the phosphate ore need to be verified by microscopic analysis.

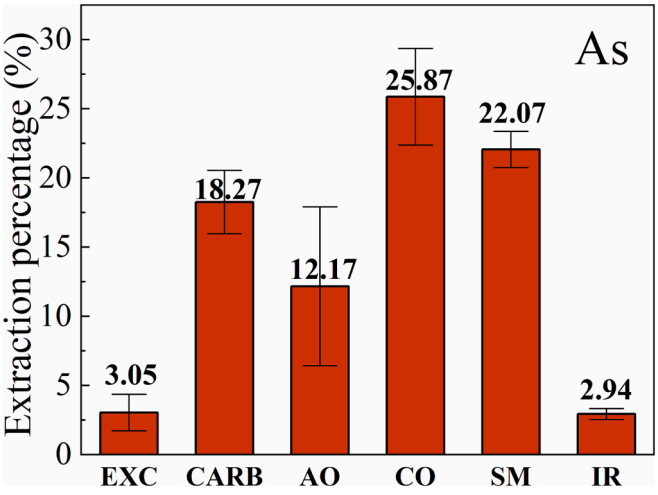


**Fig. 3.** Arsenic distribution in the phosphate ore from the SSE procedure.

**Insoluble residue fraction (IR).** The final insoluble residue solids were weighted as an average mass of 0.24 g (Table S2). The remaining As in the IR fraction was calculated as 2.94 %, while the Al and Si remaining in this fraction were approximately 50 % and 95 % (Figs. S3 and 2d), respectively. On the one hand, Al represents clay minerals, and the clay minerals in the IR fraction might contain small amounts of As probably due to the stable sequestration by clay minerals (Zhang et al., 2018). On the other hand, organic constituents in the phosphate ore were insoluble so it entirely remained in the IR fraction (Stow, 1969; Baioumy, 2005). Thus, organic matter and clay minerals might be attributed to this proportion of As.

## 3.3. Occurrence mode of arsenic in minerals

### 3.3.1. Carbonate minerals

Combined with the previous SSE results, As is possibly presented in Mn-containing carbonate minerals. To recognize these minerals, the phosphate ore slice was analyzed by TIMA as shown in Fig. 4a. The arsenic-containing mineral in the phosphate ore was identified as rhodochrosite. Combined with SEM backscatter image (Fig. 4b), rhodochrosite was symbiotic with quartz and illite, surrounded by matrix of apatite. Table 4 presents the EPMA results of compositions of the different rhodochrosite particles in the phosphate ore. The content of $As_2O_5$ in different rhodochrosite particles ranged was 0.015–0.153 % with an average $As_2O_5$ content of 0.079 % (equal to 0.052 % As). All of the rhodochrosite particles found from the microanalysis were determined to be arsenic-containing by EPMA-WDS. These results confirmed that rhodochrosite was one of the important arsenic-containing minerals in phosphate ore. The total amount of elements in the minerals exceeded 100 % because the results EPMA provided were without the amount of $CO_2$ which was analyzed by adding $CO_2$ in proportion to the rhodochrosite.

Manganese played a possible role in inducing As immobilization in calcite (Nilling et al., 2022). Rhodochrosite is a calcite-group mineral (Luo et al., 2018), which shows the same crystal structure and similar chemical composition as calcite. It could be inferred that the As in the rhodochrosite of phosphate ore might be due to the fixation of As by Mn. In addition, no As peaks were determined in dolomite (Fig. S2), and no other carbonate minerals in the phosphate ore were found during the microanalysis. These findings confirmed that the release of As in CARB fraction from SSE was from rhodochrosite dissolution.

### 3.3.2. Iron oxides/hydroxides

It was reported that As could occur in iron oxides/hydroxides (Aftabtalab et al., 2022; Bari et al., 2022), as iron oxides/hydroxides have considerable adsorption capacity for As (Zhang et al., 2004; Zhang et al., 2017; Thakur and Armstrong, 2021). The microscopic morphology and proximate As content of iron oxides/hydroxides in the phosphate ore were analyzed using TEM-EDS as shown in Fig. 5. The $As_2O_5$ contents of iron oxides/hydroxides in phosphate ores ranged from 0.127 to 0.360 %, with an average $As_2O_5$ content of 0.217 % (equal to 0.142 % As) (Table S3). The average As content in iron oxides/hydroxides is much higher than that of phosphate ore in Florida which contained a high content of 0.054 % As in the hydrous ferric oxides (Lazareva and Pichler, 2009). The iron oxides/hydroxides in the phosphate ore existed as aggregates of small acicular crystals (Fig. 5a), graininess aggregate (Fig. 5b), agglomerates on small iron oxide/hydroxide particles as botryoidal aggregates (Fig. 5c), and the inclusion of tiny particles of iron oxides/hydroxides (Fig. 5d). Additionally, the As content of iron oxides/hydroxides in phosphate ore varied with the surface morphology of iron oxides/hydroxides, as the lowest As content of 0.05 % was found in the acicular crystal iron oxides/hydroxides, and the highest As content of 0.61 % was found in the inclusions of iron oxides/hydroxides. In this study, As content appeared to increase with increasing particle size of iron oxides/hydroxides. Iron oxides/hydroxides have been extensively studied as adsorbents for As because of their

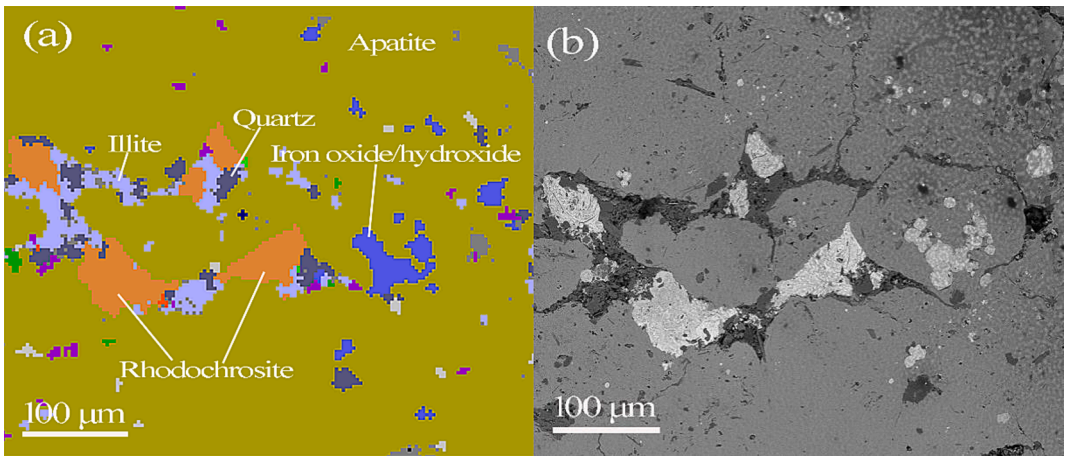


**Fig. 4.** The (a) TIMA and (b) SEM backscatter images of rhodochrosite in the phosphate ore.

**Table 4**
Compositions of different rhodochrosite particles in the phosphate ore obtained from EPMA-WDS analyses (wt%).

| No. | MnO | FeO | BaO | MgO | $Al_2O_3$ | $As_2O_5$ | CaO | $CO_2$ | Total |
|---|---|---|---|---|---|---|---|---|---|
| 1 | 50.720 | 6.821 | 5.762 | 3.034 | 3.438 | 0.127 | 2.298 | 38.290 | 110.490 |
| 2 | 54.706 | 0.075 | 5.725 | 3.802 | 2.432 | 0.039 | 2.495 | 38.290 | 107.564 |
| 3 | 56.657 | 0.44 | 6.87 | 2.483 | 0.958 | 0.039 | 2.339 | 38.290 | 108.076 |
| 4 | 54.911 | 0.427 | 6.034 | 2.650 | 1.042 | 0.098 | 2.432 | 38.290 | 105.884 |
| 5 | 35.177 | 24.52 | 4.739 | 2.175 | 2.189 | 0.153 | 1.898 | 38.290 | 109.141 |
| 6 | 56.040 | 0.349 | 8.387 | 1.466 | 0.444 | 0.015 | 2.244 | 38.290 | 107.235 |
| Average | 51.369 | 5.439 | 6.253 | 2.602 | 1.751 | 0.079 | 2.284 | 38.290 | 108.065 |

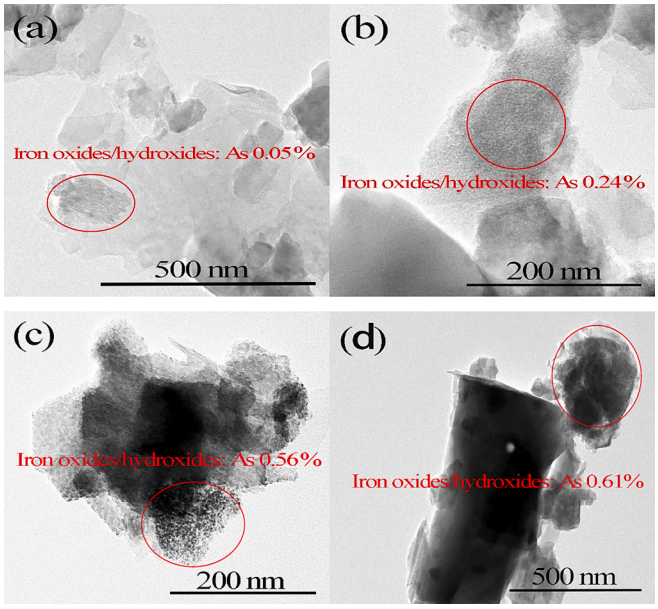


**Fig. 5.** The TEM image and arsenic content of iron oxides/hydroxides in the phosphate ore.

strong affinity for As (Fendorf et al., 1997; Yavuz et al., 2006; Yang et al., 2014; Chen et al., 2022a). Therefore, the As of iron oxide/hydroxide in the phosphate ore was most likely to be present in the form of adsorption. Previous studies have confirmed that the adsorption of As was highly dependent on the particle size of the iron oxides/hydroxides (Yean et al., 2005; Mayo et al., 2007). The kind of adsorption of As with iron oxides/hydroxides could not be released according to the SSE results. This might be responsible for the adsorption behavior that happened at the earlier stages, and the combined forms have been strong bonds during the weathering and deposition process of phosphate ore. It is worth mentioning that all the iron oxide/hydroxide particles found under the TEM observations were arsenic-containing.

Furthermore, the SEM backscatter image exhibited that the iron oxides/hydroxides in phosphate ore had different brightness, with darker areas indicating higher silicon and As content relative to the brighter sections (Fig. 6 and Table 5). Hence, there is a correlation between arsenic and silicon. In minerals, As could replace silicon since the ionic radii of $As^{5+}$ (0.46 Å) are fundamentally similar to the radius of $Si^{4+}$ (0.40 Å), making ionic substitution possible (Onishis and Sandell, 1955; Shannon, 1976). It is speculated that the As element adsorbed by iron oxides/hydroxides may have exchanged for the silicon in the iron oxides/hydroxides, thus making iron oxides/hydroxides continue to adsorb more As. This could explain why small amounts of iron oxides/hydroxides contain high silicon content and high As content simultaneously.

### 3.3.3. *Sulfide minerals*

The widespread presence of As in sedimentary sulfide minerals has been well known (Zhao et al., 2021). The previous research reported that $As^{3+}$ and $As^{1-}$ could respectively substitute for $Fe^{2+}$ and $S_2^{2-}$ in pyrite (Deditius et al., 2008). The SSE analysis results also speculated that As in phosphate ore might occur in sulfide minerals. Afterward, TEM-EDS analysis revealed massive (Fig. 7a) and spherical (Fig. 7b) pyrite particles in the phosphate ore with As content of 0.01 and 0.07 %, respectively. Pyrite in sediments was demonstrated enrichment of As with a heterogeneous distribution (Lazareva and Pichler, 2009). To find out the exact amount of As in pyrite, EPMA analysis was carried out on the phosphate ore slice as shown in Table 6. The results showed that 2 of the 12 pyrite particles did not contain As or contained less As lower than the EPMA can determine and the other 10 pyrite particles were determined as arsenic-containing ranging from 0.008 to 0.100 %, with average As content of 0.047 %. These pyrites had the potential to be generated in hydrothermal systems (Qiu et al., 2017). The total amount of elements in the pyrite was less than 100 % due to the pyrite particles

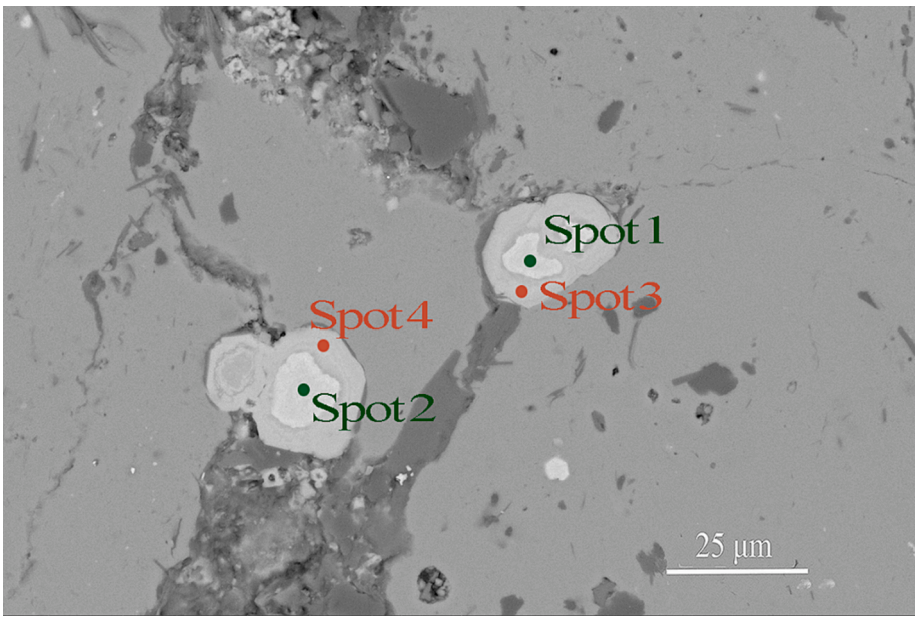


**Fig. 6.** The SEM backscatter image of the iron oxides/hydroxides in the phosphate ore.

**Table 5**
Compositions of different iron oxides/hydroxides particles in the phosphate ore obtained from EPMA-WDS analyses (wt%).

| No. | FeO | MnO | $SiO_2$ | MgO | $Al_2O_3$ | $As_2O_5$ | $K_2O$ | CaO | $P_2O_5$ | Total |
|---|---|---|---|---|---|---|---|---|---|---|
| Spot 1 | 72.620 | 0.051 | 2.443 | 0.360 | 0.225 | 0.181 | 0.030 | 1.163 | 0.157 | 77.230 |
| Spot 2 | 72.644 | 0.156 | 2.910 | 0.607 | 0.461 | 0.147 | 0.013 | 1.176 | 0.204 | 78.318 |
| Spot 3 | 64.236 | 0.233 | 8.821 | 0.664 | 2.876 | 0.360 | 0.104 | 2.163 | 0.873 | 80.330 |
| Spot 4 | 61.936 | 0.272 | 7.970 | 0.623 | 2.578 | 0.302 | 0.129 | 3.397 | 1.659 | 78.866 |

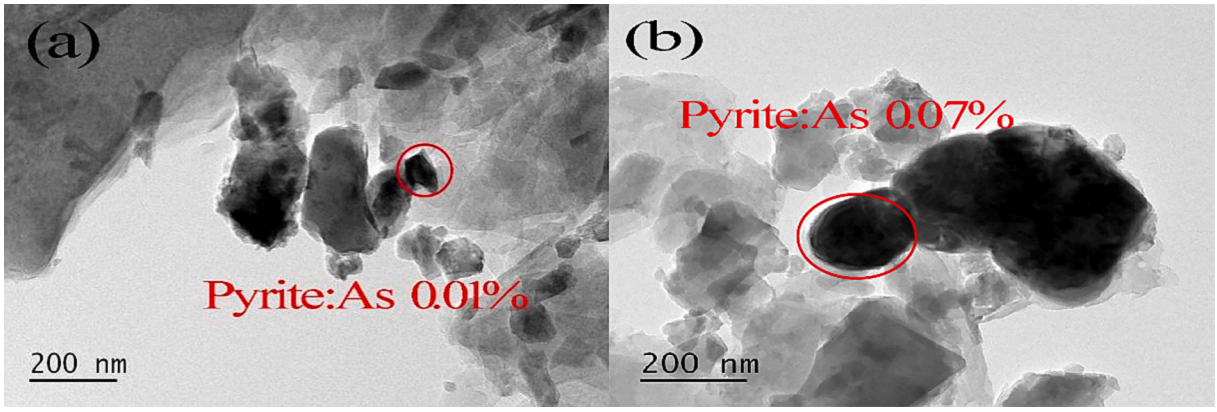


**Fig. 7.** The TEM images and arsenic content of pyrites in the phosphate ore.

in the phosphate ore being mostly smaller than 1 nm, and the EPMA electron beam would hit the impurities around the pyrite particles.

From the microanalysis, two sphalerite particles in the phosphate ore were found without arsenic-containing as shown in Table 6. It seems that As tended to substitute Fe rather than S in the sulfide minerals. Additionally, an independent As mineral in phosphate ore was identified as arsenopyrite under SEM observation as shown in Fig. 8 (EDS analysis shown in Fig. S4). The arsenopyrite particle was small and embedded in apatite. However, arsenopyrite was rarely observed in comparison with pyrite under SEM observations. Although not all pyrite contained As, pyrite phases contributed most As for sulfide minerals in the phosphate ore sample.

### 3.4. Arsenic removal analysis

Based on the above findings, As mainly existed in all of rhodochrosite, all of iron oxides/hydroxides, and parts of pyrite. According to the contents of the minerals/phases and their As contents, As amounts in the phosphate ore descended in the order of iron oxides/hydroxides > pyrite > rhodochrosite. Totally, the distribution of As was dispersed in the phosphate ore and occurred in several different mineral phases, so it is not conducive to one-step removal of As.

Beneficiation technology, especially flotation, is still widely used for removal of silicate and carbonate minerals from medium-low-grade phosphate ore (Wang et al., 2022). Since rhodochrosite is chemically similar to dolomite which can be removed by reverse flotation separation (Chen et al., 2022b), the As in rhodochrosite can probably be

**Table 6**
Compositions of different pyrites and sphalerites particles in the phosphate ore obtained from EPMA-WDS analyses (wt%).

| Mineral | No. | Fe | Mn | Mg | As | Al | Ca | P | S | Total |
|---|---|---|---|---|---|---|---|---|---|---|
| Pyrite | 1 | 39.729 | 0.308 | 0.105 | 0.060 | 0.544 | 1.124 | 0.383 | 47.772 | 90.025 |
| | 2 | 43.466 | 0.636 | 0.064 | 0.008 | 0.136 | 0.809 | 0.210 | 54.081 | 99.410 |
| | 3 | 36.343 | 0.216 | 0.193 | 0.080 | 2.231 | 0.563 | 0.163 | 45.094 | 84.883 |
| | 4 | 38.118 | 0.279 | 0.049 | 0.097 | 0.271 | 0.368 | 0.087 | 47.218 | 86.487 |
| | 5 | 38.359 | 0.344 | 0.169 | 0.100 | 0.453 | 1.003 | 0.331 | 45.542 | 86.301 |
| | 6 | 40.317 | 0.052 | 0.057 | 0.043 | 0.120 | 0.716 | 0.235 | 46.239 | 87.779 |
| | 7 | 44.385 | 0.000 | 0.012 | 0.000 | 0.095 | 0.519 | 0.118 | 51.457 | 96.586 |
| | 8 | 42.887 | 0.139 | 0.014 | 0.074 | 0.106 | 0.642 | 0.207 | 50.346 | 94.415 |
| | 9 | 38.932 | 0.029 | 0.110 | 0.000 | 0.200 | 3.790 | 1.592 | 43.680 | 88.333 |
| | 10 | 44.606 | 0.110 | 0.002 | 0.032 | 0.030 | 0.379 | 0.029 | 53.000 | 98.188 |
| | 11 | 44.740 | 0.001 | 0.004 | 0.000 | 0.026 | 0.599 | 0.109 | 53.109 | 98.588 |
| | 12 | 44.482 | 0.014 | 0.012 | 0.066 | 0.033 | 0.588 | 0.142 | 52.765 | 98.102 |
| Average | — | 41.364 | 0.177 | 0.066 | 0.047 | 0.354 | 0.925 | 0.301 | 49.192 | 92.425 |
| Mineral | No. | Fe | Zn | Ca | Si | Mg | As | S | P | Total |
| Sphalerite | 1 | 4.763 | 41.986 | 8.672 | 1.864 | 0.131 | 0.000 | 23.620 | 3.790 | 86.005 |
| | 2 | 1.132 | 57.340 | 0.905 | 0.968 | 0.190 | 0.000 | 30.916 | 0.183 | 92.630 |

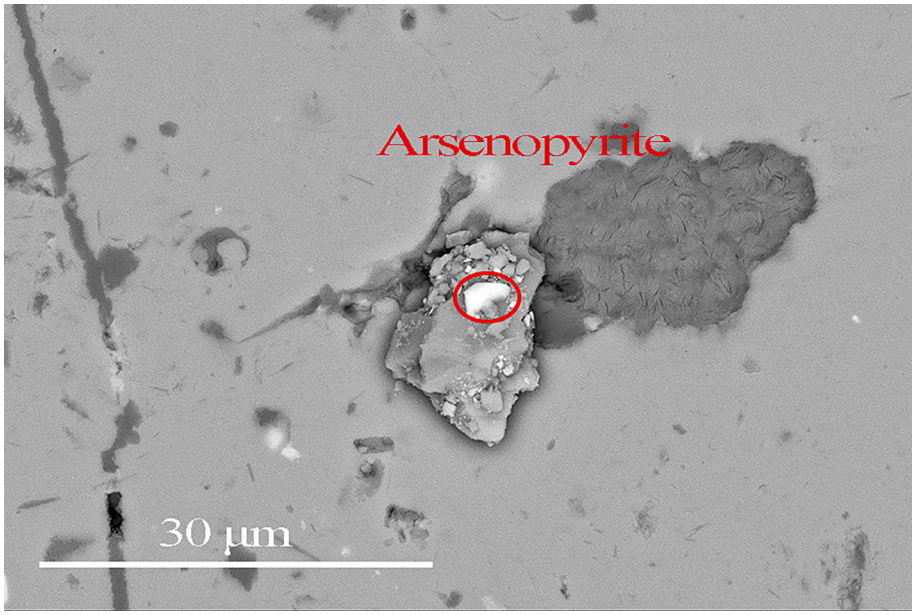


**Fig. 8.** The SEM image of arsenopyrite found in the phosphate ore.

removed in flotation process. For example, increasing the amount of flotation agent can lower the carbonates contents in the flotation concentrate by controlling the Mn contents. The removal of As from phosphate ore can be achieved by inhibiting iron oxides/hydroxides by adding starch inhibitors during direct flotation of phosphate ore (Wang et al., 2023). In fact, iron oxides/hydroxides have been regarded as one of the toxic components during the phosphate ore flotation process, and according to the current findings, the content of iron oxides/hydroxides in phosphate ore concentrate can be lowered to concurrently decrease As. In terms of As in pyrite, it should be difficult to be removed or separated by flotation due to the small size of pyrite particles (Fig. 1b). Probably, additional chemical beneficiation can be employed for removal of the As in pyrite.

## 4. Conclusions

The mineral composition of the phosphate ore used in this study was determined as apatite, dolomite, and quartz, with small amounts of others, such as pyrite, iron oxides/hydroxides. Accordingly, its chemical composition of $P_2O_5$, CaO, and $SiO_2$ accounted respectively for 24.10, 36.40, and 18.96 wt%. The As content in the phosphate ore was 43.8 mg/kg, which would be enriched in the downstream phosphorus chemical products. Selective sequential extraction procedure was conducted to reveal the As distribution in different fractions. The results showed that As in the total oxides/hydroxides fraction accounted for approximately 38 %, followed by sulfate fraction minerals (22.07 %) and carbonate minerals (18.27 %) fraction. Moreover, 3.05 % of As was extracted as an exchangeable and soluble fraction during the sequential extraction procedure. Correspondingly, microanalysis of TEM-EDS, SEM-EDS, and EPMA-WDS verified that iron oxides/hydroxides, rhodochrosite, and pyrite were the main arsenic-containing minerals/phases, with the average As contents of 0.142, 0.052, and 0.047 %, respectively. All of the oxides/hydroxides and rhodochrosite particles found from the microanalysis were determined arsenic-containing, while a large proportion of the pyrite particles contained As and a small number of pyrite particles did not contain As. Consequently, As amounts in the phosphate ore descended in the order of iron oxides/hydroxides > pyrite > rhodochrosite. These minerals/phases could be removed by different beneficiation methods, such as flotation and chemical minerals processing.

## CRediT authorship contribution statement

**Guiyong Zhou:** Investigation, Resources, Data curation, Writing –

original draft. **Ning Wang:** Conceptualization, Resources, Supervision. **Wei Xu:** Resources. **Guotao Hu:** Resources. **Hannian Gu:** Writing – review & editing, Conceptualization, Validation, Resources, Methodology, Supervision, Funding acquisition.

## Declaration of Competing Interest

The authors declare that they have no known competing financial interests or personal relationships that could have appeared to influence the work reported in this paper.

## Data availability

Data will be made available on request.

## Acknowledgments

The work was financially supported by the Youth Innovation Promotion Association CAS, China (2021400) and Guizhou Outstanding Young Scientific and Technological Talents Project (2021-5641).

## Appendix A. Supplementary material

Supplementary data to this article can be found online at https://doi.org/10.1016/j.mineng.2023.108363.

## References

Aarab, I., Derqaoui, M., El Amari, K., Yaacoubi, A., Abidi, A., Etahiri, A., Baçaoui, A., 2021. Influence of surface dissolution on reagents' adsorption on low-grade phosphate ore and its flotation selectivity. Colloids Surf. A Physicochem. Eng. Asp. 631, 127700. https://doi.org/10.1016/j.colsurfa.2021.127700.

Aftabtalab, A., Pinklebe, J., Shaheen, S.M., Niazi, N.K., Moreno-Jiménez, E., Schaller, J., Knorr, K.-H., 2022. Review on the interactions of arsenic, iron (oxy)(hydr)oxides, and dissolved organic matter in soils, sediments, and groundwater in a ternary system. Chemosphere 286, 131790. https://doi.org/10.1016/j.chemosphere.2021.131790.

Bahsaine, K., Mekhzoum, M.E.M., Benzeid, H., Qaiss, A., Bouhfid, R., 2022. Recent progress in heavy metals extraction from phosphoric acid: A short review. J. Ind. Eng. Chem. 115, 120–134. https://doi.org/10.1016/j.jiec.2022.08.029.

Baioumy, H.M., 2005. Preliminary data on cadmium and arsenic geochemistry for some phosphorites in Egypt. J. Afr. Earth Sc. 41, 266–274. https://doi.org/10.1016/j.jafrearsci.2005.03.002.

Bari, A.F., Lamb, D., MacFarlane, G.R., Rahman, M.M., 2022. Soil washing of arsenic from mixed contaminated abandoned mine soils and fate of arsenic after washing. Chemosphere 296, 134053. https://doi.org/10.1016/j.chemosphere.2022.134053.

Benredjem, Z., Delimi, R., 2009. Use of extracting agent for decadmiation of phosphate rock. Phys. Procedia 2 (3), 1455–1460. https://doi.org/10.1016/j.phpro.2009.11.116.

Chen, T., Ji, M., Wen, L., Guo, T., Pan, S., Cheng, S., Lu, Z., Pan, B., 2022a. In-situ forming Sub-2 nm hydrous iron oxide particles in MOFs for deep-treatment and high anti-interference in arsenic removal. Chem. Eng. J. 431, 113813 https://doi.org/10.1016/j.cej.2021.133813.

Chen, J., Yuan, X., Yin, Y., Wang, M., Cheng, D., Ao, X., Xie, Y., 2022b. Effect of $Ca^{2+}$ dissolution and migration transformation from phosphorite on the surface properties of dolomite. Miner. Eng. 188, 107824 https://doi.org/10.1016/j.mineng.2022.107824s.

Curran, R., Lopez, J., 2021. US Environmental Protection Agency: Petition for rulemaking: Phosphogypsum and process wastewater from phosphoric acid production. Available online: https://www.epa.gov/sites/default/files/2021-02/documents/phosphogypsum_and_process_wastewater_petition_for_rulemaking.pdf (accessed on 26 August 2023).

Dai, S., Li, D., Ren, D., Tang, Y., Shao, L., Song, H., 2004. Geochemistry of the late Permian No. 30 coal seam, Zhijin Coalfield of Southwest China: Influence of a siliceous low-temperature hydrothermal fluid. Appl. Geochem. 19, 1315–1330. https://doi.org/10.1016/j.apgeochem.2003.12.008.

Daryani, M., Jodeiri, N., Fatehifar, E., Shahbazi, J., 2022. Optimization of operating conditions in purification of wet process phosphoric acid in a liquid-liquid extraction column. Chem. Eng. Commun. 209 (8), 1082–1095. https://doi.org/10.1080/00986445.2021.1946520.

Deditius, A., Utsunomiya, S., Renock, D., Ewing, R.C., Ramana, C.V., Becker, U., Kesler, S.E., 2008. A proposed new type of arsenian pyrite: Composition, nanostructure and geological significance. Geochim. Cosmochim. Acta 72, 2919–2933. https://doi.org/10.1016/j.gca.2008.03.014.

Dong, L., Wei, Q., Jiao, F., Qin, W., 2021. Utilization of polyepoxysuccinic acid as the green selective depressant for the clean flotation of phosphate ores. J. Clean. Prod. 282, 124532 https://doi.org/10.1016/j.jclepro.2020.124532.

Doušová, B., Lhotka, M., Grygar, T., Machovič, V., Herzogová, L., 2011. In situ co-adsorption of arsenic and iron/manganese ions on raw clays. Appl. Clay Sci. 54, 166–171. https://doi.org/10.1016/j.clay.2011.08.004.

Elser, J.J., 2012. Phosphorus: a limiting nutrient for humanity? Curr. Opin. Biotechnol. 23 (6), 833–838. https://doi.org/10.1016/j.copbio.2012.03.001.

Fendorf, S., Eick, M.J., Grossl, P., Sparks, D.L., 1997. Arsenate and chromate retention mechanisms on goethite. 1. Surface structure. Environ. Sci. Tech. 31 (2), 315–320. https://doi.org/10.1021/es950653t.

Gál, P., Polgári, M., Józsa, S., Gyollai, I., Kovács, I., Szabó, M., Fintor, K., 2020. Contribution to the origin of Mn-U-Be-HREE-enrichment in phosphorite, near Bükkszentkereszt. NE Hungary. Ore Geology Reviews 125, 103665. https://doi.org/10.1016/j.oregeorev.2020.103665.

Goren, O., 2015. Distribution and mineralogical residence of trace elements in the Israeli carbonate oil shales. Fuel 143, 118–130. https://doi.org/10.1016/j.fuel.2014.11.024.

Islam, M.S., Maamoun, I., Falyouna, O., Eljamal, O., Saha, B.B., 2023. Arsenic removal from contaminated water utilizing novel green composite Chlorella vulgaris and nano zero-valent iron. J. Mol. Liq. 370, 121005 https://doi.org/10.1016/j.molliq.2022.121005.

Jiang, J., 2014. Way for the development and utilization of medium-low grade phosphate rock. Multipurpose Utilization of Mineral Resources. 04, 16–19 (In Chinese with English abstract).

Lazareva, O., Pichler, T., 2009. Naturally occurring arsenic in the Miocene Hawthorn Group, southwestern Florida: Potential implication for phosphate mining. Appl. Geochem. 22, 953–973. https://doi.org/10.1016/j.apgeochem.2006.12.021.

Li, S., Ge, Y., Fang, J., 2020. Experimental study on arsenic removal from industrial phosphoric acid. Ind. Minerals Process. 49 (02), 24–26. https://doi.org/10.16283/j.cnki.hgkwyjg.2020.02.007 (In Chinese with English abstract).

Liu, J., Ward, C.R., Graham, I.T., French, D., Dai, S., Song, X., 2018. Modes of occurrence of non-mineral inorganic elements in lignites from the Mile Basin, Yunnan Province, China. Fuel 222, 146–155. https://doi.org/10.1016/j.fuel.2018.02.124.

Luo, N., Wei, D., Shen, Y., Liu, W., Gao, S., 2018. Effect of calcium ion on the separation of rhodochrosite and calcite. J. Mater. Res. Technol. 7 (1), 96–101. https://doi.org/10.1016/j.jmrt.2017.04.007.

Mayo, J.T., Yavuz, C., Yean, S., Cong, L., Shiple, H., Yu, W., Falkner, J., Kan, A., Tomson, M., Colvin, V.L., 2007. The effect of nanocrystalline magnetite size on arsenic removal. Sci. Technol. Adv. Mater. 8 (1–2), 71–75. https://doi.org/10.1016/j.stam.2006.10.005.

Mirlean, N., Medeanic, S., Garcia, F.A., Travassos, M.P., Baisch, P., 2012. Arsenic enrichment in shelf and coastal sediment of the Brazilian subtropics. Cont. Shelf Res. 35, 129–136. https://doi.org/10.1016/j.csr.2012.01.006.

Ni, S., Jin, B., Zhong, W., 1997. A preliminary study on the As content in Lower Cambrian phosphorite of east Yunnan. Yunnan Geology 16 (03), 272–275 (In Chinese with English abstract).

Nilling, J., Verma, A., Singh, A., 2022. Precipitation of arsenic-bearing solids as a secondary control on arsenic speciation in groundwater: Evidence from field study and geochemical analysis. Geochim. Cosmochim. Acta 333, 308–332. https://doi.org/10.1016/j.gca.2022.07.017.

Onishis, H., Sandell, E., 1955. Geochemistry of arsenic. Geochim. Cosmochim. Acta 7, 1–33. https://doi.org/10.1016/0016-7037(55)90042-9.

Qiu, G., Gao, T., Hong, J., Tan, W., Liu, F., Zheng, L., 2017. Mechanisms of arsenic-containing pyrite oxidation by aqueous arsenate under anoxic conditions. Geochim. Cosmochim. Acta 217, 306–319. https://doi.org/10.1016/j.gca.2017.08.030.

Ren, H., Yang, R., Gao, J., Cheng, W., Wei, H., 2015. Enrichment regularities for iodine concentration in phosphorite of Doushantuo Formation of Late Ediacaran in Guizhou Province, SW China. Arab. J. Geosci. 8, 5423–5437. https://doi.org/10.1007/s12517-014-1604-7.

Shannon, R.D., 1976. Revised effective ionic radii and systematic studies of interatomic distances in halides and chalcogenides. Acta Crystallogr. A 32, 751–767. https://doi.org/10.1107/S0567739476001551.

Stow, S.H., 1969. The occurrence of arsenic and the color-causing components in Florida land-pebble phosphate rock. Econ. Geol. 64 (6), 667–671. https://doi.org/10.2113/gsecongeo.64.6.667.

Tessier, A., Campbell, P.G.C., Bisson, M., 1979. Sequential extraction procedure for the speciation of particulate trace metals. Anal. Chem. 51, 844–851. https://doi.org/10.1021/ac50043a017.

Thakur, A., Armstrong, D.W., 2021. Arsenic sequestration by iron oxide coated geopolymer microspheres. J. Clean. Prod. 291, 125931 https://doi.org/10.1016/j.jclepro.2021.125931.

USGS, 2022. Mineral Commodity Summaries. Phosphate Rock. 124–125 https://doi.org/10.3133/mcs2022.

Wang, B., Luo, K., 2014. Preparation and research advance of electronic grade phosphoric acid. Adv. Mater. Res. 881–883, 71–73. https://doi.org/10.4028/www.scientific.net/AMR.881-883.70.

Wang, B., Zhou, Z., Xu, D., Wu, J., Yang, X., Zhang, Z., Yan, Z., 2022. A new enrichment method of medium-low grade phosphate ore with the high silicon content. Miner. Eng. 181, 107548 https://doi.org/10.1016/j.mineng.2022.107548.

Wang, Q., Zhang, Y., Xu, Y., Bao, S., Liu, C., Yang, S., 2023. The molecular structure effects of starches and starch phosphates in the reverse flotation of quartz from hematite. Carbohydr. Polym. 303, 120484 https://doi.org/10.1016/j.carbpol.2022.120484.

Wen, R., 1992. Requirements for chemicals and high-purity water used in large-scale integrated circuits. Chemical Reagents 14 (01), 20–24. https://doi.org/10.13822/j.cnki.hxsj.1992.01.008 (In Chinese with English abstract).

Wenzal, W.W., Kirchbaumer, N., Prohaska, T., Stingeder, G., Lombi, E., Adriano, D.C., 2001. Arsenic fractionation in soils using an improved sequential extraction

procedure. Anal. Chim. Acta 436, 309–323. https://doi.org/10.1016/s0003-2670(01)00924-2.

Wu, F., Zhao, C., Qu, G., Liu, S., Ren, Y., Chen, B., Li, J., Liu, L., 2022. A critical review of the typical by-product clean ecology links in the Chinese phosphorus chemical industry in China: Production technologies, fates and future directions. J. Environ. Chem. Eng. 10 (2), 106685. https://doi.org/10.1016/j.jece.2021.106685.

Yang, B., Guan, Z., 2023. Upgrading silicon-calcareous phosphate ores using sodium polymer [(Naphthalene formaldehyde) sulfonate] (PNFS) as an efficient and eco-friendly depressant. Miner. Eng. 197, 108075 https://doi.org/10.1016/j.mineng.2023.108075.

Yang, Y., Wu, Y., Zhang, H., Zhang, M., Liu, Q., Yang, H., Lu, J., 2016. Improved sequential extraction method for determination of alkali and alkaline earth metals in Zhundong coals. Fuel 181, 951–957. https://doi.org/10.1016/j.fuel.2016.05.014.

Yang, J., Zhang, H., Yu, M., Emmanuelawati, I., Zou, J., Yuan, Z., Yu, C., 2014. High-content, well-dispersed γ-$Fe_2O_3$ nanoparticles encapsulated in macroporous silica with superior arsenic removal performance. Adv. Function Material 24 (10), 1354–1363. https://doi.org/10.1002/adfm.201302561.

Yavuz, C.T., Mayo, J.T., Yu, W.W., Prakash, A., Falkner, J.C., Yean, S., Cong, L., Shipley, H.J., Kan, A., Tomson, M., Natelson, D., Colvin, V.L., 2006. Low-field magnetic separation of monodisperse $Fe_3O_4$ nanocrystals. Science 314 (5801), 964–967. https://doi.org/10.1126/science.1131475.

Yean, S., Cong, L., Yavuz, C.T., Mayo, J.T., Yu, W., Falkner, J.C., Kan, A.T., Colvin, V.L., Tomson, M.B., 2005. Effect of magnetite particle size on adsorption and desorption of arsenite and arsenate. J. Mater. Res. 20 (12), 3255–3264. https://doi.org/10.1557/jmr.2005.0403e.

Zhang, X., Cheng, C., Qian, J., Lu, Z., Pan, S., Pan, B., 2017. Highly efficient water decontamination by using sub-10 nm FeOOH confined within millimeter-sized mesoporous polystyrene beads. Environ. Sci. Tech. 51 (16), 9210–9218. https://doi.org/10.1021/acs.est.7b01608.

Zhang, W., Singh, P., Paling, E., Delides, S., 2004. Arsenic removal from contaminated water by natural iron ores. Miner. Eng. 17, 517–524. https://doi.org/10.1016/j.mineng.2003.11.020.

Zhang, Y., Tian, J., Feng, S., Yang, F., Lu, X., 2018. The occurrence modes and geologic origins of arsenic in coal from Santanghu Coalfield, Xinjiang. J. Geochem. Explor. 186, 225–234. https://doi.org/10.1016/j.gexplo.2017.12.006.

Zhao, Y., Zhao, H., Abashina, T., Vainshtein, M., 2021. Review on arsenic removal from sulfide minerals: An emphasis on enargite and arsenopyrite. Miner. Eng. 172, 107133 https://doi.org/10.1016/j.mineng.2021.107133.